Molecular dynamics simulations of the meltinglike transition in $Li_{13}Na_{42}$ and $Na_{13}Cs_{42}$ clusters

Andrés Aguado* and José M. López
Departamento de Física Teórica, Universidad de Valladolid, Valladolid 47011, Spain
(Received 27 September 2004; revised manuscript received 12 November 2004; published 22 February 2005)

Equilibrium geometries and the meltinglike transition of $Na_{13}Cs_{42}$ and $Li_{13}Na_{42}$ are studied by means of orbital-free density-functional-theory molecular dynamics simulations. A polyicosahedral structure is found to be energetically favored for $Na_{13}Cs_{42}$, with a core shell formed by Na atoms and complete segregation of Cs atoms to the cluster surface. $Li_{13}Na_{42}$ adopts an amorphouslike structure, albeit with significant local polyicosahedral order, with the Na atoms preferentially occupying surface sites but with partial mixing of Li and Na species at the cluster core. Analysis of the thermal properties reveals that premelting effects are more important for heterogeneous than for homogeneous alkali clusters. The nature of these premelting effects is discussed in detail. For $Na_{13}Cs_{42}$, they involve isomerizations without significant atom diffusion; for $Li_{13}Na_{42}$, they also include partial melting of the surface formed by Na atoms. The mixing of Li and Na species is significantly enhanced above the melting temperature, while surface segregation of Cs in $Na_{13}Cs_{42}$ is maintained in the liquid state. From the study of these two clusters, we attempt to extract some general trends about the structural and thermal behaviors of heterogeneous alkali clusters.

DOI: 10.1103/PhysRevB.71.075415 PACS number(s): 31.15.Qg, 36.40.Ei, 36.40.Sx, 64.70.Dv

I. INTRODUCTION

Chemically heterogeneous metallic clusters (or nanoalloys) constitute a fascinating subject of research for many reasons. From the experimental side, metal nanoparticles may have physical and chemical properties not observed in bulk systems, like enhanced catalytic activity.[1] For bulk systems, alloying of two metals may result in ordered intermetallic phases with *genuine* properties (which cannot be obtained as a simple average of properties of the separate species). In a similar way, nanoalloys will present different chemical reactivity depending on the concentration and degree of surface segregation, mixing, etc. Also, some metals that present a miscibility gap at the bulk level may be miscible at the nanoscale level, opening interesting possibilities such as the synthesis of new materials.

From the theoretical side, heterogeneous clusters show a much richer structure in their isomer energy spectra than homogeneous clusters. Here it is convenient to distinguish between topological and permutational isomers.[2] Topological isomers differ in the geometric arrangement of atoms, irrespective of the chemical identity of those atoms. (For example, icosahedra, cuboctahedra, and decahedra form families of topologically distinct isomers). Permutational isomers, on the other hand, differ just in the relative positions of different atoms within a given geometric structure. Jellinek and Krissinel[3] have introduced the term "homotop" to refer to these permutational isomers. Now, permutation of the positions of any two atoms in a homogeneous cluster does not lead to a new isomer. On the contrary, a permutation of atomic positions involving different species will normally result in a new isomer, depending on the specific symmetry of the underlying topological geometry. (Two different homotops will not usually share exactly the same atomic positions, due to small relaxation effects induced by differences in size, bonding, etc., of the atomic species involved.) The number of homotops increases with the number of atoms N as 2^N for bimetallic clusters, which superimposes to the approximately exponential increase in the number of topological isomers to lead to an extremely rich density of states in configurational phase space. This added complexity is expected to confer specific structural, thermal, and electronic properties to heterogeneous clusters.

The lowest energy structure (both topological and permutational) of a heterogeneous cluster is determined by a competition between several effects, usually interconnected but not in a simple, intuitive, way. The relative bond strengths of the atomic species involved, the size mismatch effects, the minimization of the strain energy accumulated in the inner part of the cluster, and the different surface tensions of the elements forming the cluster are all factors that conjointly determine the segregation/mixing preferences (the most favorable homotop for each isomeric structure) as well as the specific geometry of the cluster. For example, Rossi *et al.*[4] have recently shown that alloying of two noble metals stabilizes core-shell poly-icosahedral structures such as the compact anti-Mackay structure of $Ni_{13}Ag_{32}$. This structure contains an Ag_{32} anti-Mackay overlayer surrounding a Ni_{13} icosahedral core. The anti-Mackay overlayer itself is formed by 20 Ag atoms in hcp positions plus 12 Ag atoms capping the vertex positions of the inner icosahedron, as opposed to a Mackay overlayer, which is formed by 30 atoms in fcc positions plus 12 atoms in vertex positions. Anti-Mackay overlayers are not specially stable for homogeneous noble metal clusters because the strain in the inner 13-atom icosahedron is very large, but they are very stable in the mixture because both core (Ni) and surface (Ag) atoms have interatomic distances close to optimal.

The same effects influence in an important way the thermal properties of nanoalloys. When different homotops of a given inherent structure have similar binding energies, solid-solid transformations between them may occur at low temperatures as precursors of the meltinglike transition.[5,6] For example, if a segregated structure is the most stable at low temperatures, an entropically driven transition towards a structure with compositional disorder may be observed be-

fore melting.[7] The occurrence of solid-solid transformations will depend, however, on the time of observation, because these processes may be governed by very slow kinetics if the transformation pathways connecting different homotops involve the surmounting of large free energy barriers. This happens when the topography of the potential energy surface (PES) has a multiple-funnel character. Here, a funnel is defined as a set of downhill pathways on the PES which ultimately drive the system to a specific low energy minimum. Once the cluster is trapped in a given funnel, it takes a very long time for it to overcome the free-energy barriers which lead to a different funnel. In computer simulations of the thermal properties of heterogeneous clusters the quasiergodic hypothesis is thus at question, and several Monte Carlo (MC)–based schemes have been developed in order to efficiently sample the configurational phase space available at each temperature and thus obtain meaningful averages for thermodynamic properties.[5–7] In molecular dynamics (MD) simulations, on the contrary, some of those solid-solid transformations will not be accessible for reasonable time lengths (of the order of nanoseconds), as different regions of phase space are essentially disconnected at low energies. Time averaging of microscopic properties obtained in an MD run may therefore pertain to the domain of kinetics for low energies, and a different sequence of transformations (as compared to MC runs) may be observed upon heating the cluster, depending on the dynamically accessible structures.[3] MD is nevertheless a very convenient tool as it allows one to follow the time evolution of the system and analyze in detail the mechanisms of melting for specific isomers.

The multiple-funnel character of the potential energy landscape has another important consequence; location of the ground state structure is an extremely difficult task, much more difficult than in the homogeneous case. Recent efforts in locating minimum-energy structures of bimetallic clusters, modeled with phenomenological potentials, have employed genetic algorithms,[8] with promising results.

Most of the theoretical work on heterogeneous metal clusters has been devoted to structural properties. López *et al.*[9] studied the segregation properties of Na-Cs and Na-Li nanoalloys of several compositions through static calculations. Similar studies were carried out by Bol *et al.*[10] on binary Na-K and ternary Na-K-Cs clusters. *Ab initio* calculations, such as those of Deshpande *et al.*[11] on Na-Li, Joshi and Kanhere[12] on Li-Sn, and Chacko *et al.*[13] on Al-Li clusters, are restricted to small sizes, while consideration of structural preferences in larger bimetallic clusters is usually performed by modeling with phenomenological potentials.[4,8] There are also a few MD simulations on bimetallic clusters which consider their freezing[14] and melting[2,12,15,16] transitions and the influence of temperature on segregation.[17] Very recently, Aguado *et al.*[18,19] have performed MD simulations of melting in the impurity-doped alkali clusters A_1Na_{54}, with A=Li, K, Rb, and Cs, and in the nanoalloy $Cs_{12}Na_{43}$. There it was found that substitution of a single Na atom in Na_{55} with a different alkali atom, while preserving the icosahedral symmetry of the ground state isomer, is enough to alter the melting properties, as reflected in the different temperatures for activation of diffusive motion of atoms of each species. For $Cs_{12}Na_{43}$, we identified a solid-solid transition, from a phase in which the Cs atoms are well mixed with Na surface atoms to another one with completely segregated Cs surface atoms. This is indeed the opposite behavior of the order-disorder transition found by Vicéns and López.[7] The reasons for such "anomalous" thermal behavior were analyzed in those works.[19] In order to gain better understanding and draw some conclusions about the systematics of melting in bimetallic clusters, it is necessary to explicitly analyze further examples. In this paper, we report the results of extensive MD simulations of the meltinglike transition in $Li_{13}Na_{42}$ and $Na_{13}Cs_{42}$. We keep the total number of atoms equal to 55 in order to make contact with our previous work. As we will show, a specificity of these clusters is that the ground state structure is not icosahedral anymore, but polyicosahedral for $Na_{13}Cs_{42}$ and amorphouslike (albeit with significant local order) for $Li_{13}Na_{42}$. The interplay between segregation and mixing properties and topological structure will affect the thermal properties of both clusters in different ways.

The rest of the paper is structured as follows: Section II presents a brief summary of our theoretical method, a full account of which can be found in our recent publications.[19] Section III describes our (necessarily approximate) strategy to locate minimum-energy isomers and an extensive analysis of the MD simulations of cluster melting. Finally, Sec. IV offers some concluding remarks.

II. THEORY

For a given spatial configuration of atoms, we evaluate the energy of the cluster and the force acting on each atom by employing density functional theory (DFT) in its Hohenberg-Kohn[20] (HK) representation where the valence electron density stands as the basic variable, thus avoiding employment of auxiliary one-particle orbitals as in its Kohn-Sham[21] (KS) representation. The details of our implementation of this so-called orbital-free DFT scheme have been described in previous work,[18,19,22–25] so we just present briefly the main technical issues. The electronic kinetic energy functional of the electron density is approximated by the gradient expansion around the homogeneous limit through second order.[20,26–28] This means that we keep the local Thomas-Fermi term and the lowest order density gradient correction. The local density approximation is used for exchange and correlation.[29,30] The ionic field acting on the electrons is represented by the local pseudopotential of Fiolhais *et al.*[31] We have shown in recent publications,[18,19] by explicit comparison of HK- and KS-DFT calculations, that the orbital-free level of theory is adequate to study alkali clusters. This conclusion may not apply to more complex metallic elements, for which an extension either of the electronic kinetic energy functional or the local pseudopotential might be needed.

The cluster under study is placed in a unit cell of a cubic superlattice with edge 62 a.u. and the set of plane waves periodic in that superlattice, up to an energy cutoff of 20 Ry, is used as a basis set to expand the valence electron density. Following Car and Parrinello,[32] the coefficients of that expansion are regarded as generalized coordinates of a set of fictitious classical particles, and the corresponding Lagrange

equations of motion for the electron density distribution are solved in order to determine the optimal electron density for each atomic configuration, as described in Ref. 19. Forces on atoms are then evaluated by using Hellmann-Feynman's theorem. Thus the dynamics of ions is not Car-Parrinello, but Born-Oppenheimer. Fourier transforms are calculated on a $144\times144\times144$ mesh, and the fictitious mass associated with the electron density coefficients is 2.4×10^7 a.u. The equations of motion are integrated using the Verlet algorithm[33] for both electrons and ions, with time steps of 1×10^{-4} atu and 3×10^{-3} atu for the electronic and ionic motions, respectively. These choices resulted in a conservation of the total energy better than 0.1%. Several MD runs at different constant energies were performed in order to obtain the caloric curve for each cluster. Previous to each constant-energy run, isokinetic thermalization runs were performed to fix the average value of the temperature. The total simulation time was at least 100 ps for each run at constant energy, but for those energies close to the meltinglike transition, some runs longer than 200 ps were performed. The total simulated time for each cluster was close to 2 ns.

A number of different indicators were employed in order to analyze the meltinglike transition. First, the average internal temperature T is defined from the equipartition theorem for the average kinetic energy,

$$T=\frac{2\langle E_k\rangle}{3N-6}, \tag{1}$$

where we have taken into account the fact that the position of the center of mass of the cluster was fixed and the total angular momentum was held to zero during the simulations, thus reducing the number of degrees of freedom from $3N$ to $3N-6$. The thermodynamic definition of temperature in the microcanonical ensemble, T_{mc}, is given by the slope of the entropy function, $1/T_{mc}=(\partial S/\partial E)_{N,V}$. This definition is equivalent to the internal temperature defined above if we take the entropy to be $S=k_B\Omega(N,V,E)$, where k_B is Boltzmann's constant and $\Omega(N,V,E)$ is the phase space *volume*.[34] That is, from such an entropy definition the equipartition theorem may be derived. If, on the contrary, we take as our definition of entropy $S=k_B\omega(N,V,E)$, where $\omega(N,V,E)$ is the phase space *density*, then T_{mc} differs from our internal cluster temperature by terms proportional to N^{-1} (Ref. 35). Nevertheless, for the cluster sizes considered in this work both entropy definitions are equivalent in practical terms, and the corresponding temperature differences are smaller than our statistical precision.

A second indicator is the specific heat per particle (in units of the Boltzmann constant),

$$C_v=\left[N-N\left(1-\frac{2}{3N-6}\right)\langle E_{kin}\rangle_t\langle E_{kin}^{-1}\rangle_t\right]^{-1}. \tag{2}$$

Our definitions of temperature and specific heat are the same as those derived by Pearson *et al.*[34] from general thermodynamic arguments, with the only difference being the number of degrees of freedom. Therefore, the previous equation recovers the correct low temperature limit for the specific heat of a classical harmonic system, namely, $C_v/(3N-6)k_B=1$, as well as the correct $N\to\infty$ limit.

The rest of melting indicators are (a) the root-mean-squared bond-length fluctuation,

$$\delta=\frac{2}{N(N-1)}\sum_{i<j}\frac{\sqrt{\langle R_{ij}^2\rangle_t-\langle R_{ij}\rangle_t^2}}{\langle R_{ij}\rangle_t}, \tag{3}$$

where R_{ij} is the distance between atoms i and j; (c) the diffusion coefficient of atoms of species A,

$$D_A=\frac{1}{6}\frac{d}{dt}\langle r_A^2(t)\rangle, \tag{4}$$

which is obtained from the long time behavior of the corresponding mean square displacement $\langle r_A^2(t)\rangle=1/N_An_t\Sigma_{j=1}^{n_t}\Sigma_{i=1}^{N_A}[\vec{R}_i(t_{0_j}+t)-\vec{R}_i(t_{0_j})]^2$, where n_t is the number of time origins, t_{0_j}, considered along a trajectory, and N_A the number of atoms of species A; (d) short-time averages of the "atomic equivalence indexes,"[36]

$$\sigma_i(t)=\sum_j|\vec{R}_i(t)-\vec{R}_j(t)|; \tag{5}$$

and (e) the microcanonical average of the atomic distribution function, defined by

$$dN_{at}(r)=g(r)dr, \tag{6}$$

where $dN_{at}(r)$ is the number of atoms at distances from the center of mass between r and $r+dr$.

III. RESULTS

A. Lowest energy isomers

To find the ground state isomer of a 55-atom cluster is an extremely difficult task. Efficient global optimization techniques such as genetic[8,37] or basin hopping[38] algorithms have been employed to locate putative global minimum structures for metal clusters when a phenomenological model for atomic interactions is assumed. On the contrary, when the potential energy landscape is sampled by DFT means, the number of energy evaluations required by either genetic or basin hopping algorithms becomes prohibitive. Therefore, in practical terms, we are forced to employ an approximate method of sampling of the potential energy landscape.

We have chosen a combination of previously gathered knowledge about the structure of metal clusters and dynamical simulated annealing to locate an isomer which is at least reasonably close to the real ground state structure. Specifically, simulated annealing runs were performed, starting from a liquid cluster equilibrated at 200 K, at a cooling rate of 0.2 K/ps, which means a simulation length of 1 ns takes the cluster to 0 K. In practice, we rather stopped the annealing simulation at 5 K and then performed a conjugate gradients optimization of the resulting structure. We also considered isomers constructed by hand with icosahedral, decahedral, and cuboctahedral symmetries, which are between the expected topological structures for metal clusters. For each of these isomers, we additionally performed a mild

annealing simulation by heating the cluster to approximately 100 K (in any case, a temperature lower than the melting point) and cooling it down at a rate of 0.4 K/ps. In many cases, this has the effect of locating an isomer of the same symmetry as the original one but with a slightly lower energy.

In the construction of isomers with icosahedral, decahedral, and cuboctahedral structures, we initially assumed that the atomic species with higher surface tension and smaller size (Li in $Li_{13}Na_{42}$ and Na in $Na_{13}Cs_{42}$) prefer to avoid the surface of the cluster. This is the expected behavior and has indeed been observed to be the case in previous studies.[9,10,18] Thus, taking as an example the icosahedral case and $Na_{13}Cs_{42}$, we started from a perfect Na_{13} icosahedral seed and studied which is the most favorable way of covering this icosahedron with Cs atoms. We did this by adding one atom at a time, and found that Cs atoms always prefer to sit on the faces (anti-Mackay growing) rather than on the edges (Mackay growing) of Na_{13}. Anti-Mackay growing has previously been found to be favorable even for homogeneous metal clusters in the initial stages of covering of the icosahedral core.[39] Here it is energetically favorable until the icosahedral core is fully covered, which leads to a geometric shell closing for $Na_{13}Cs_{32}$ (the 32 Cs atoms are split into two nonequivalent groups of atoms: 20 Cs atoms on the 20 faces of Na_{13} plus 12 Cs atoms capping the pentagonal faces of the resulting dodecahedron). Similar considerations employing decahedral and cuboctahedral Na_{13} seeds always led to higher-energy isomers. The same trends were observed for the growing of Na over a Li_{13} core shell. Therefore, from this point we disregarded both decahedral and cuboctahedral isomers and just studied which is the most favorable way of adding ten more Cs atoms to the $Na_{13}Cs_{32}$ anti-Mackay structure. The first Cs atom preferred to sit on a face of $Na_{13}Cs_{32}$, but for larger numbers of Cs atoms, a complex combination of face and edge covering was observed. In all cases, the energetic ordering of isomers was the same for mixed Li-Na clusters.

Figures 1 and 2 show some of the minimum energy isomers found for $Na_{13}Cs_{42}$ and $Li_{13}Na_{42}$, respectively. In the ground state isomer of $Na_{13}Cs_{42}$, the ten Cs atoms in the most external surface shell try to attain an optimal packing, and to this end the neighboring face and edge sites of the underlying $Na_{13}Cs_{32}$ are occupied. A more symmetrical isomer, with all ten Cs atoms lying on face sites of $Na_{13}Cs_{32}$, is only 0.9 meV/atom higher in energy. In isomer (c) of Fig. 1, two anti-Mackay umbrellas[39] are capping diametrically opposed pentagonal pyramids of $Na_{13}Cs_{32}$. Finally, isomer (d) of Fig. 1 was obtained from a simulated annealing run from the liquid. It lies just 2.3 meV/atom higher than the ground state and, more interestingly, shows the same $Na_{13}Cs_{32}$ complete anti-Mackay structure. It differs from the other three structures just in the way the ten Cs atoms of the outermost shell are allocated. This implies that the simulated annealing method is quite efficient in this case in locating good approximations to the minimum energy structure, and that the anti-Mackay icosahedral structure of $Na_{13}Cs_{32}$ is also kinetically favored. The energetic ordering of these isomers can be easily rationalized in terms of well known features of metallic bonding, namely, isomer (a) is the one with the largest number of Cs-Cs bonds and the shortest average Cs-Cs distance.

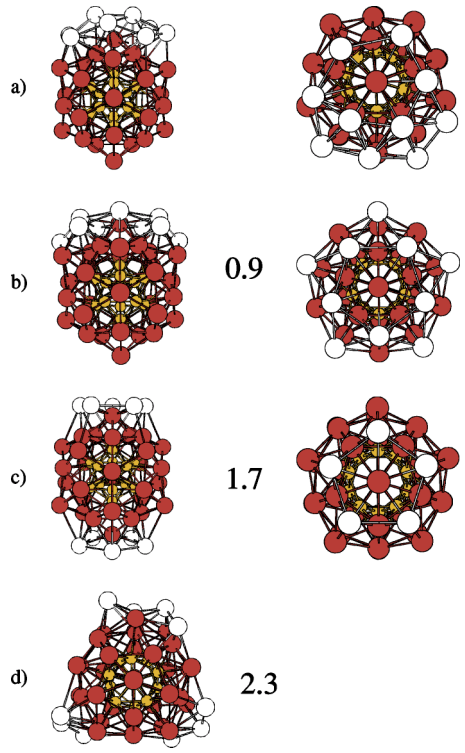

FIG. 1. (Color online) Lowest energy structure and low-lying isomers of $Na_{13}Cs_{42}$. Side and top views are offered on left and right columns, respectively. Small light (yellow) balls represent Na atoms, and large dark (red) balls represent the 32 Cs atoms completing the 45-atom compact anti-Mackay structure, while large white balls represent the ten Cs atoms in the outermost shell. Numbers are energy differences with respect to the ground state isomer (a) in meV/atom.

Let us turn our attention now to Fig. 2, which shows the three lowest energy isomers found for $Li_{13}Na_{42}$. The first thing to notice is that all the isomers shown in Fig. 1 are not especially stable for $Li_{13}Na_{42}$, even though they were found to be stable after the mild annealing procedure from 100 K, explained above. The ground state isomer [Fig. 2(a)] was found instead by simulated annealing from the liquid state. It has an inner shell formed by 16 atoms, with stoichiometry $Li_{13}Na_3$, which is a 13-atom icosahedron with three additional atoms capping three neighboring faces (again anti-Mackay growing). Interestingly, one of the Li atoms of the 13-atom icosahedron has been substituted with a Na atom, indicating a stronger tendency for mixing than observed in Na-Cs nanoalloys. The 13-atom icosahedron is distorted, with the vertex Na atom displaced from its fivefold edge of symmetry. (This is most clearly seen in the top view.) This way, all the triangular faces of the icosahedron do not have the same area, and the two other Na atoms are precisely capping the two faces with the largest surface areas. This core structure has 26 faces in total, 24 of which are capped by Na atoms of the external shell, which demonstrates that anti-Mackay growing is still favorable energetically. The remaining 15 Na atoms are capping the 12 pentagons of the outer anti-Mackay shell and three edges. Due to the "imper-

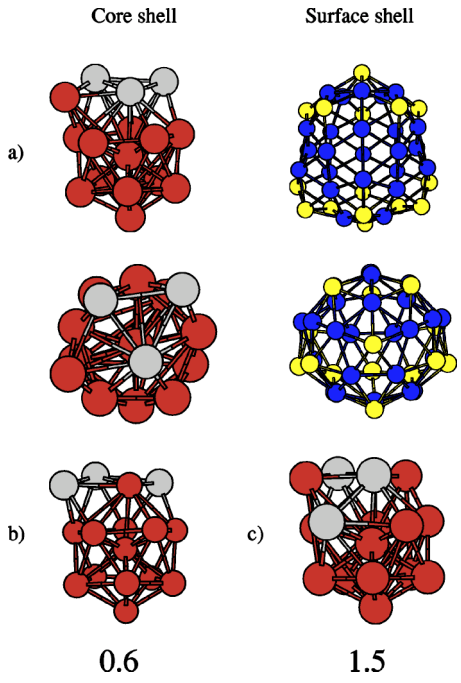

FIG. 2. (Color online) Lowest energy structure and low-lying isomers of $Li_{13}Na_{42}$. For the ground state isomer (a), both the core and surface shells, in two different views, are offered. In the core shell, dark (red) and light (gray) balls represent Li and Na atoms, respectively. In the surface shell, dark (blue) balls represent those Na atoms capping the faces of the core shell, and light (yellow) spheres represent the rest of the surface Na atoms. For higher energy isomers, only the core shell is shown as the surface shell is unchanged except for slight distortions. Numbers are energy differences with respect to the ground state isomer (a) in meV/atom.

fect" structure of the core shell of atoms, the ground state structure of $Li_{13}Na_3$ looks quite amorphous if not displayed by concentric shells (as shown in Fig. 2) and is also amorphous in terms of the distribution of interatomic distances, which is quite spread. Nevertheless, Fig. 2 shows that there is substantial local order in this structure, which is dictated by a preference towards anti-Mackay growing. In isomer (b), the core shell is a Li_{13} icosahedron with three Na atoms capping neighboring faces, and it lies 0.6 meV/atom higher in energy. Finally, isomer (c), which lies 1.5 meV/atom above the ground state, demonstrates that substitution of two Li atoms by Na atoms in the 13-atom icosahedron is already unfavorable, so the tendency towards mixing is very weak, in agreement with previous calculations.[9]

Polyicosahedral structures in binary metal clusters have been independently identified by Rossi *et al.*[4] for the case of noble metals. In homogeneous clusters, this growing pattern accumulates a very large strain in the inner 13-atom icosahedron and thus is not usually observed. In a binary *AB* nanoalloy, on the contrary, the atomic species with the shortest equilibrium interatomic distance and/or higher surface tension (*A*) may form the inner A_{13} icosahedral core with little or no accumulated strain. At the same time, *A*-*B* interatomic distances and packing of *B* atoms can both be optimized by anti-Mackay growing because only 20 faces (as opposed to 30 edges) need to be capped. As Rossi *et al.* point out, particularly stable polyicosahedral structures are expected whenever the differences in surface energies and atomic sizes of the species involved are sufficiently large. In this work, we have shown this to be the case for Na-Cs nanoalloys. On the contrary, Na and Li atoms are more similar, and segregation of the species with lower surface tension is not so marked, which slightly reduces the stability of polyicosahedral structures.

The acquiring of an amorphous structure is now a well established mechanism for stabilization of some metallic nanostructures, and it has been documented for pure gold,[37] sodium,[24,40] platinum[41] and zinc and cadmium[38] clusters. In all these studies, it was stressed that the amorphous clusters possess an appreciable local order, even though the broad distribution of interatomic distances resembles that of a bulk glass. The amorphization mechanism usually involves the formation of a core-shell with more than 13 atoms. For example, both Soler *et al.*[37] and Manninen *et al.*[40] report the observation of concentric atomic core shells containing "1 +14" atoms, as compared to the "1+12" structure in a perfect icosahedron. Increasing the number of atoms in the first radial shell relaxes the strain in the interior part of the cluster, as the radius of the first shell is now larger. The inner strain being smaller, the cluster may be further stabilized by contraction of the surface shell bonds. The whole process results in a better satisfaction of coordination-bond length correlations; namely, those metal atoms with lower coordination prefer to have shorter interatomic distances. In this work, we have found that these amorphization mechanisms can also play a role in bimetallic clusters, at least when the two species involved do not have a strong preference for segregation. In the case of $Li_{13}Na_{42}$, a "1+15" core shell is found. As Na and Li are not too dissimilar atoms, some mixing is allowed to form a bigger core shell. As a result, a second atomic shell (surface shell) is enough to cover the core, contrary to the situation found in $Na_{13}Cs_{42}$ where the 42 Cs atoms form two atomic shells on top of Na_{13}. This can be accomplished because Na and Li atoms have similar sizes and the Na atoms have on average a lower coordination than Li atoms, which makes the distribution of distances more homogeneous across the cluster. In summary, the amorphous structure optimizes packing (maximum number of bonds) without the need for very short interatomic distances (strain) in the inner part of the cluster.

To close this section, we would like to emphasize that we do not claim to have found the global minimum for $Li_{13}Na_{42}$ and $Na_{13}Cs_{42}$ because our search has not been extensive. Nevertheless, the energetic ordering of the isomers presented here is preserved by orbital-based KS-DFT calculations performed with the SIESTA code,[42] under the same approximation for exchange-correlation effects and with core electrons substituted by norm-conserving pseudopotentials[43] in their fully nonlocal form.[44] This explicitly demonstrates, as in our previous works,[18,19] that the orbital-free DFT technique provides an accurate representation of atomic interactions in alkali clusters. Also, the ground state structures shown in Figs. 1 and 2 are stable against mild annealing from a temperature of 100 K, and no isomers with significantly lower energy were found in the heating runs reported in the next sections. (If lower energy isomers were sampled, this would be ob-

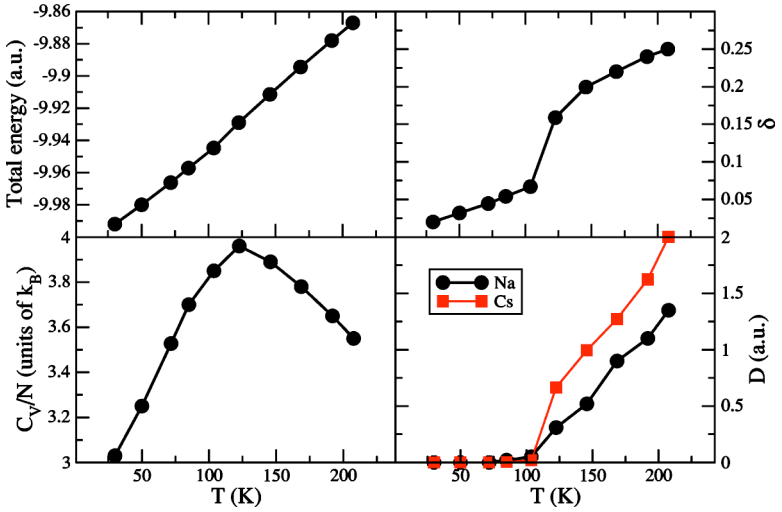

FIG. 3. (Color online) Caloric and specific heat curves (left side), and rms bond length fluctuation and diffusion constants (right side) of $Na_{13}Cs_{42}$, taking the internal cluster temperature as the independent variable.

served as a signature in the caloric curves.) Thus, the structures proposed are really good candidates for the minimum energy structures. (If an isomer with significantly lower energy exists, it must lie on a completely different funnel of the potential energy landscape, separated from the icosahedral funnel by free energy barriers sufficiently high that complete melting of the cluster is needed before the new funnel can be explored.)

B. Meltinglike transition in $Na_{13}Cs_{42}$

Figure 3 shows the caloric curve, as well as the temperature evolution of the specific heat, rms bond length fluctuation, and diffusion constants. All the indicators agree in locating the melting temperature at $T_m \approx 125$ K. The specific heat departs significantly, however, from the value corresponding to a cold, harmonic solid for temperatures lower than T_m, while the diffusion constants are zero within our statistical accuracy, and δ takes values typical of a solid cluster, where only atomic vibrations about the equilibrium positions are expected. This is suggestive of the presence of nondiffusive isomerizations for $T < T_m$. This would explain the quite broad peak in the specific heat, as the configurational phase space volume available to the cluster would increase with temperature in a progressive, as opposed to sudden, way.

Figure 4 shows the radial atomic density distributions at several average temperatures, and Fig. 5 shows short-time averages of the atomic equivalence indexes for $T = 85$ K. Both of these figures will be helpful in analyzing the nature of the melting process, but in order to have a complete view, a direct inspection of the MD trajectories using computer graphics is necessary. At $T = 71$ K, the Cs atoms are clearly distributed into two surface shells. The inner one comprises 32 atoms, as discussed in the previous section, and can be further subdivided into two groups of 20 and 12 atoms each. [The minimum in $g(r)$ separating these two subshells is not exactly zero due to thermal fluctuations.] The outermost surface shell contains ten surface atoms. At this temperature, the isomerizations do not involve any interchange of atomic positions, but just temporary excursions of, for example, a Cs atom of the outermost surface shell from a face to an edge position. After such a temporary excursion, the atom comes back to its original position, so these processes can be alternatively viewed as very large amplitude vibrations and do not increase much the values of δ or the diffusion coefficient.

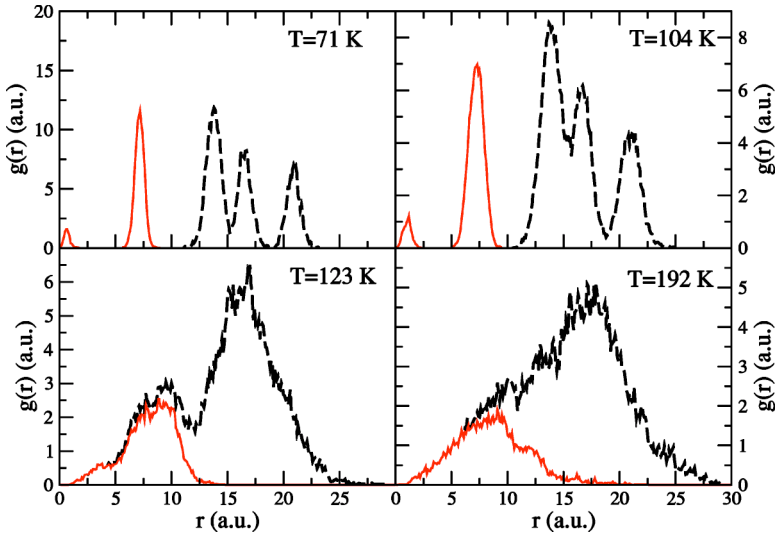

FIG. 4. (Color online) Time-averaged radial atomic density distributions (dashed lines) of $Na_{13}Cs_{42}$, at some representative temperatures. The full line is the contribution of Na atoms to $g(r)$. Where both lines coincide, only the full line is displayed.

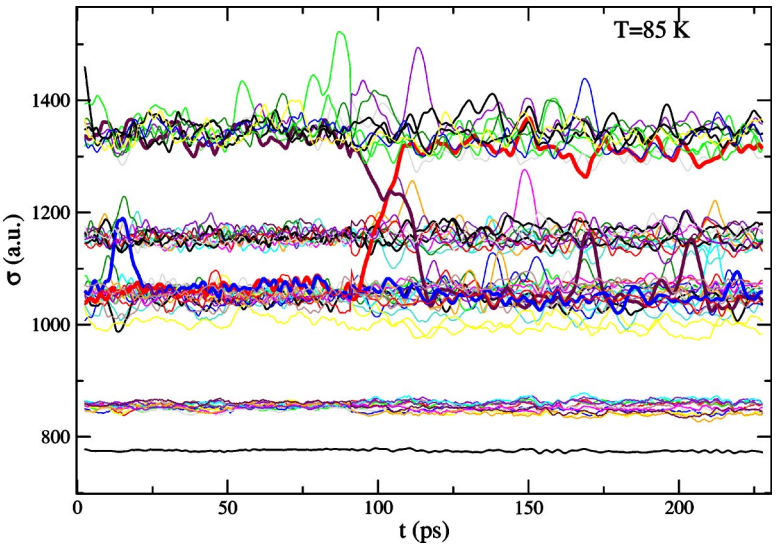

FIG. 5. (Color online) Time evolution of atomic equivalence indexes of $Na_{13}Cs_{42}$, averaged over time intervals of 1000 steps, at $T=85$ K. Some of the σ curves corresponding to Cs atoms involved in isomerization transitions are represented by bold lines.

Usually these isomerization processes involve not the displacement of a single atom, but the concerted motion of several atoms. Specific isomerizations may be identified by first looking at the atomic equivalence indexes, which are very sensitive indicators of structural changes and tell us which atoms are involved in isomerizations, and then watching those atoms move in an MD movie. The isomerizations which do not involve the swapping of atomic positions are identified in Fig. 5 as those lines which significantly depart from their average value during just a short time interval. From the three boldface σ curves in Fig. 5, one is representative of this situation. This particular line has an average value corresponding to a Cs atom sitting on a face of the inner Na_{13} icosahedron and temporarily takes values typical of the 12 vertex atoms in the same inner surface shell. During such a time interval, that atom continues to sit on a face on the inner Na_{13} icosahedron, but is coordinated just to five surface atoms instead of six, resulting in a larger σ value. Armed with this equipment, we are thus in a position to analyze every isomerization process in detail.

At a higher temperature of 104 K, Fig. 4 shows that there is some mixing between the two surface shells. Figure 5 shows that, starting at a temperature of 85 K, some interchanges between the two surface shells appear which explain the features in $g(r)$. Specifically, this process was observed just once in the 85 K simulation (which was longer than 200 ps) and more frequently as the temperature is raised from that value. By inspecting the movie, the two Cs atoms that interchange radial shells are never found to be in neighboring sites, so the process is not a simple swapping of atomic positions. (This would have been identified as a strong increase in δ, for example.) The isomerization, rather, involves a concerted movement of atoms which resembles a shear elastic wave at the cluster surface. This way new isomers may be visited without atomic diffusion and without significant bond breaking.

Upon further heating, homogeneous melting is observed at 123 K (Fig. 4). The surface shell is not structured anymore, but the mixing of core and surface shells is still quite impeded kinetically. At a higher temperature of 192 K, even the distinction between core and surface shells is washed out, and atoms are more uniformly distributed across the cluster. In the liquid state, some slight penetration of Cs atoms into the core region is observed, but, on average, segregation of Cs atoms to the cluster surface is maintained for all temperatures.

The melting process in $Na_{13}Cs_{42}$ thus involves activation of three different mechanisms. (a) In the temperature interval $T \approx 50-80$ K, isomers other than the ground state may be visited just by temporary excursions of some atoms to neighboring sites. These atoms always come back to their original positions afterwards. (b) For $T \approx 80-120$ K, isomerizations may change the distribution of atoms in the different surface shells. (c) At $T \approx 125$ K, homogeneous melting, involving substantial atomic diffusion and bond breaking occurs. It is in this sense that the melting process can be considered to proceed stepwise, even though just one broad peak in the specific heat is observed. While the two first processes cannot be clearly located by typical structural (δ) and dynamical (D) indicators, an examination of atomic equivalence indexes helps in identifying the relevant physical mechanisms. When homogeneous melting sets in, considerable exploration of configurational phase space has been already achieved by means of the first two processes (premelting effects); the opening of phase space at T_m is not too abrupt, and so the specific heat peak is quite broad. Also, as Cs surface segregation is mostly maintained in the liquid state, there is not an important contribution of the entropy of mixing to the latent heat of fusion.

C. Meltinglike transition in $Li_{13}Na_{42}$

We show the information regarding the melting of $Li_{13}Na_{42}$ in Figs. 6–8, in an analogous way to that employed for $Na_{13}Cs_{42}$. In this case, the specific heat shows a marked peak at $T_m \approx 170$ K, which correlates quite well with the abrupt increase in the average of bond length fluctuations, located at about 150 K. The diffusion constant of Na atoms, however, starts to deviate from zero at an approximate temperature of 100 K. As observed for $Na_{13}Cs_{42}$, the specific heat increases appreciably for temperatures lower than T_m. Also, at a temperature slightly higher than 200 K, a small

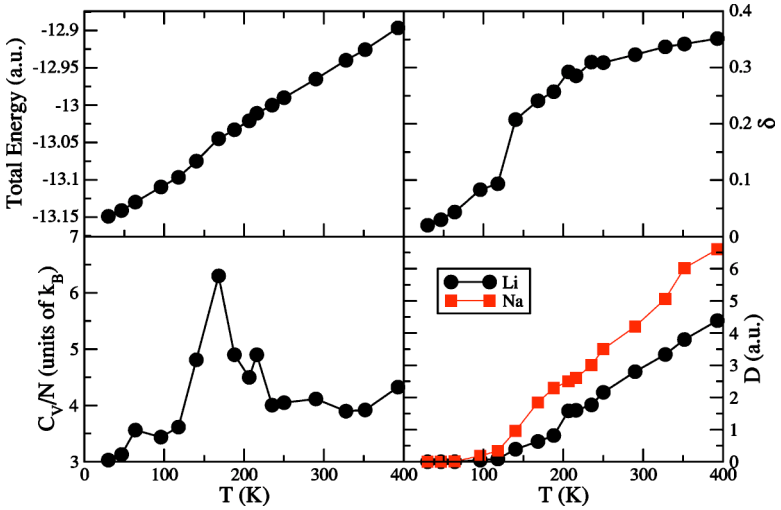

FIG. 6. (Color online) Caloric and specific heat curves (left side) and rms bond length fluctuation and diffusion constants (right side) of $Li_{13}Na_{42}$, taking the internal cluster temperature as the independent variable.

additional specific heat peak is observed which correlates with an increase in the diffusion coefficient of Li atoms. The situation is thus apparently more complex than that found in $Na_{13}Cs_{42}$.

Figure 7 shows the radial atomic density distribution at 47 K, when the cluster is still completely solid. There is a clear separation between core and surface shells, although with some Na atoms contributing to $g(r)$ in the core region. Within each shell, the distribution of distances to the center of mass is quite spread, due to the distorted core structure. At a temperature of 64 K, Fig. 8(a) shows that the original distribution of atoms in shells is still preserved, but with substantial isomerizations taking place, which results in an appreciable increase in the specific heat. These isomerizations are of the same kind as observed for $Na_{13}Cs_{42}$ and will not be further described.

Starting at ≈96 K (see Fig. 7), a new stage in the melting process develops. The distribution of radial distances in the core and surface shells is now much smoother due to the strong thermal fluctuations, but at the same time two subshells can be distinguished in the core shell. This situation persists up to 120 K, and Fig. 8(b) clearly shows that the new peak in $g(r)$ is formed by two atoms, so that the distribution of atoms in the core shell changes from "1+15" to "1+13+2." An examination of MD snapshots reveals that those two atoms are Li atoms, and that a solid-solid transformation to isomers of type (c) in Fig. 2 has taken place. As the number of Li-Na bonds (and so the mixing of the two atomic species) increases, we expect the free energy difference between isomers (a) and (c) to decrease with increasing temperature. Thermal expansion also plays a role, as we have checked that the energy difference between those isomers decreases with a homogeneous scaling of the coordinates of all particles. This observation suggests that mixing of the two species will be more favored the larger the free volume available per atom. Figure 8(b) also shows that the surface shell disorder has considerably increased. In fact, the diffusion coefficient of Na atoms starts to deviate from zero at these temperatures, which demonstrates that there is a partial melting of the cluster surface. The diffusion mechanism is illustrated graphically in Fig. 9. From time to time along the MD run, a basal edge of one of the pentagonal pyramids forming the surface opens up appreciably and leaves enough space for a neighboring atom (white ball in Fig. 9) to enter. At the

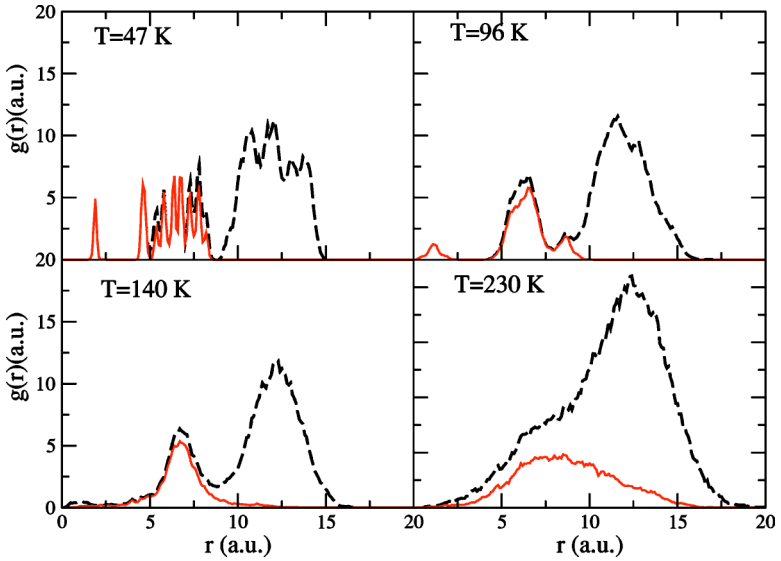

FIG. 7. (Color online) Time-averaged radial atomic density distributions (dashed lines) of $Li_{13}Na_{42}$, at some representative temperatures. Full lines represent the contribution of Li atoms to $g(r)$.

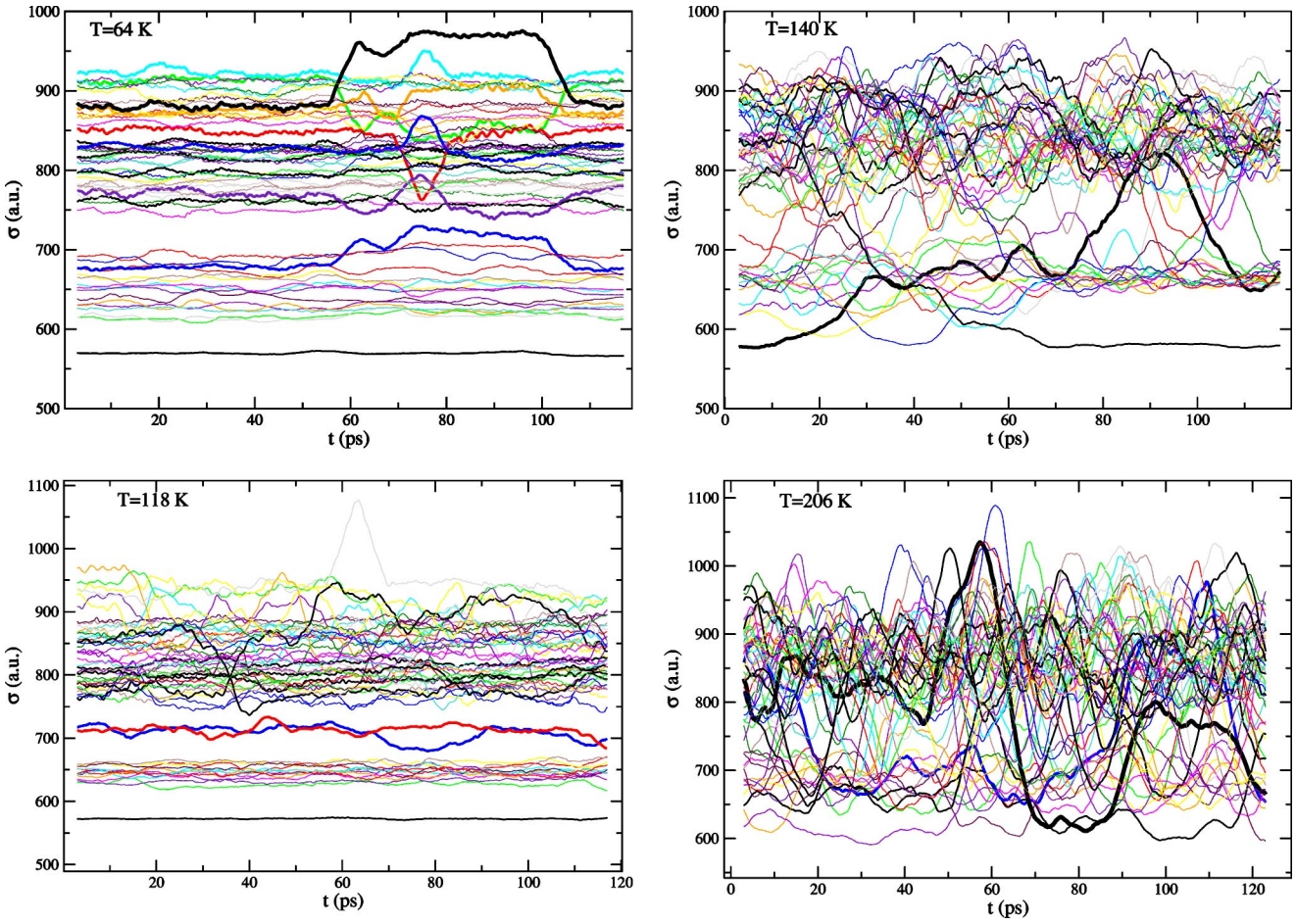

FIG. 8. (Color online) Time evolution of atomic equivalence indexes of $Li_{13}Na_{54}$, averaged over 1000 time steps, at four representative temperatures. Some σ curves are represented by bold lines in order to better appreciate signatures of isomerizations and/or diffusive motion.

same time, another atom leaves the base of the original pyramid. This transition is not reflected in the specific heat, but only in the diffusion constant and, to a lesser extent, in the magnitude of bond length fluctuations, which is close to 10%.

At $T \approx 140$ K, where an abrupt increase in the specific heat, δ, and diffusion constants appears, Figs. 7 and 8(c) show that both core and surface shells are melted, but diffusion of atoms between both shells is still relatively infrequent and mixing of Li and Na is almost unchanged. Upon increasing the temperature further, however, the radial distribution of atoms becomes much more uniform, and substantial mixing of the two species is observed [Figs. 7 and 8(d)]. This is, in our opinion, the reason for observing the main specific heat peak at a temperature higher than 140 K. Also, the small bump at ≈ 210 K correlates with an increase in the frequency with which Li atoms visit surface sites, which also explains the increase in average Li diffusion.

IV. SUMMARY AND DISCUSSION

In this paper, orbital-free DFT molecular dynamics simulations have been employed in order to analyze the mechanisms of melting in two binary alkali metal clusters, namely $Li_{13}Na_{42}$ and $Na_{13}Cs_{42}$. Ideally, what one would like to identify in these kinds of studies are some trends in the structural and thermal behavior of binary alkali clusters as a function of cluster size, composition, etc., which would be useful in developing some intuition regarding the expected behavior of related systems. Unfortunately, the computational expense of these calculations does not allow an explicit consideration of a large number of systems, a problem that can only be addressed by employing phenomenological models of atomic interactions. Orbital-free DFT remains, however, as the method which gives the best compromise between statistical accuracy and realistic interatomic forces, and some very general trends can be already identified from our restricted set of calculations.

The lowest-energy structures of binary alkali clusters of medium size are dictated by the same general features of metallic bonding which operate in homogeneous clusters, namely, the relief of core strain and the tendency of surface bonds to contract. When the two atomic species have significantly different sizes and surface energies, these "rules" lead to polyicosahedral clusters (with segregation of the lower surface energy component to the cluster surface) in a natural way, as shown in this work and independently by Rossi *et al.*[4] for the case of binary noble metal clusters. No significant strain is accumulated in the core shell of these structures as

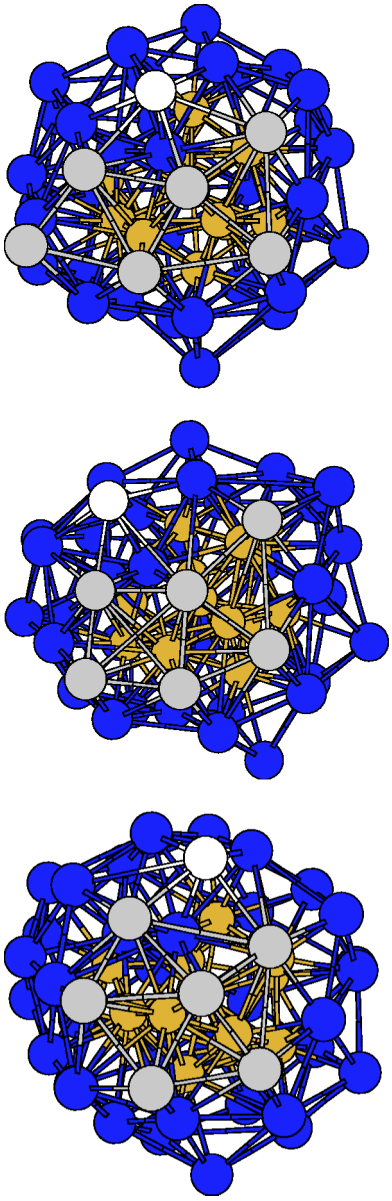

FIG. 9. (Color online) Three snapshots of $Li_{13}Na_{42}$, extracted from a MD run at 118 K, showing the surface melting mechanism at that temperature. A group of six atoms forming a pentagonal pyramid on the cluster surface is represented by light-colored (gray) balls. The white ball represents a Na atom which substitutes for one of the Na atoms initially in that pentagonal pyramid.

the smaller size species has a shorter equilibrium bond distance. At the same time, optimal distances for the surface bonds may be obtained by growing of the large size species on the faces of the inner icosahedron. (Growing on edge sites would result in surface bonds which are too short.) We have performed selected additional calculations (only trying the set of isomers shown in Figs. 1 and 2) which demonstrate that poly-icosahedral structures are also favorable for $Li_{13}K_{42}$ and $Na_{13}Rb_{42}$, for example. When the two atomic species are more similar in size and surface energy, there is some tendency towards mixing (that is, segregation is not so significantly favored), and the amorphization mechanism, also observed in homogeneous clusters,[24,37,38,40,41] can play an important role. Inner strain is relaxed by increasing the number of atoms in the core shell, which results in a larger average interatomic distance in this region, and thus contraction of the surface bonds generates a lower strain than with a 13-atom core shell. In this work, we have found that Li—Na nanoalloys present this tendency towards amorphization. Both Aguado *et al.*[24] and Manninen *et al.*[40] have reported significant local icosahedral order in amorphous Na clusters. Similarly, the "amorphous" $Li_{13}Na_{42}$ isomer shown in Fig. 2 possesses significant polyicosahedral local order, as most Na atoms on the surface shell sit on top of the triangular faces of the core shell structure. This local order is again a manifestation of the same mechanisms operating in Na-Cs nanoalloys.

Let us discuss now some general trends observed in the thermal properties of heterogeneous alkali clusters. These trends may not apply to those clusters having a compact geometric structure, like $Na_{13}Cs_{32}$, which have not been covered in this study. A first point to notice, both in this and previous works,[18,19] is that premelting effects start to be important at lower temperatures, as compared with the homogeneous case.[22–25] The premelting effects may include partial melting of the surface (as is the case for $Li_{13}Na_{42}$, where Na surface atoms undergo diffusive motions for $T<T_m$) or nondiffusive isomerizations, which in turn may or may not involve a redistribution of atoms within the different radial shells. The preponderance of premelting effects in heterogeneous alkali clusters might be related to the enhanced density of states in their isomer energy spectra. In any case, the specific nature of the premelting effects seems to be quite difficult to guess without an explicit simulation of a large number of clusters.

The premelting effects may lead to quite broad specific heat peaks, because the transition is spread over a wide temperature interval, and the configurational phase space volume available to the system increases in a more or less gradual way across that temperature interval. This is the case for the melting of $Na_{13}Cs_{42}$. $Li_{13}Na_{42}$, on the contrary, shows, apart from the premelting effects, a marked specific heat peak characteristic of an abrupt transition. This is somewhat surprising as the structure of this cluster has been classified as amorphouslike, and both Aguado *et al.*[24] and Manninen *et al.*[40] have reported tiny latent heats of fusion in amorphous Na clusters. It should be remembered here that a cluster structure has been classified in previous works[37,40] as "amorphouslike" when the distribution of interatomic distances is spread over a wide interval, and thus it resembles that found in a bulk glass. In Ref. 24 we proposed that a structurally amorphous cluster should satisfy an additional condition, namely, the probability per unit area of finding an atom at a certain radial distance r [as measured by $g(r)/4\pi r^2$] should be constant, or, put in different words, there should not be a discernible radial order. Only in this case is it observed that the melting transition proceeds with negligibly small latent heat.[24] It is clear then that $Li_{13}Na_{42}$ is not completely amorphous from a structural point of view. Now, even for a structurally amorphous heterogeneous cluster, an appreciable latent heat is expected if the cluster is not compositionally amorphous and melting is accompanied by substantial mixing of the atomic species forming the cluster. This is exactly

what happens with $Li_{13}Na_{42}$, thus providing an explanation for the high specific heat peak. Regarding the melting temperature values, they are simply close to (but slightly below) those typical of homogeneous clusters of the majority component,[23–25] but in this respect our calculations are clearly insufficient to discuss the dependence of T_m on composition.

A few comments about the quasiergodicity of the MD simulations presented in this paper are pertinent here. As mentioned in the Introduction, this is a more delicate question for heterogeneous than for homogeneous clusters, because some solid-solid transformations between energetically close homotops may be difficult to observe in MD if large energy barriers separate the corresponding energy basins. In the case of $Na_{13}Cs_{42}$, we believe our MD simulations are not worse in this respect than for a typical homogeneous cluster, because there is complete surface segregation of Cs atoms. Even at the highest energies considered (very close to the evaporation limit), we find that Cs atoms never visit the inner region of the cluster. We tried to optimize some structures with an inner Na atom substituted by an external Cs atom, and their energies were always higher than those obtained by quenching from MD trajectories at the highest temperatures. Quasiergodicity, is thus not a big problem because different homotops have very different energies. The situation is different in Li—Na nanoalloys, where surface segregation of Na is not so marked, and some energetically competitive isomers with inner Na atoms exist. In this case, however, energy barriers separating different homotops are not expected to be significantly higher than those in pure Na or Li clusters as these two atomic species are not too dissimilar, and the quasiergodicity problem is again partially alleviated. We are in fact able to locate a solid-solid transformation between homotops in $Li_{13}Na_{42}$, with simulation times not longer than 200 ps.

ACKNOWLEDGMENTS

This work was supported by Junta de Castilla y León (Project No. VA073/02) and DGES (Project No. MAT2002-04393-C02-01). Thanks are due to J. M. Soler and his team for providing us with a copy of the SIESTA code, and to M. J. López for helping us with the construction of icosahedral, cuboctahedral, and decahedral geometries. A. Aguado also acknowledges financial support from the Spanish Ministry of Science and Technology, under the Ramón y Cajal program.

*Email address: aguado@metodos.fam.cie.uva.es

[1] M. Huruta, Catal. Today **36**, 153 (1997).
[2] M. J. López, P. A. Marcos, and J. A. Alonso, J. Chem. Phys. **104**, 1056 (1996).
[3] J. Jellinek and E. B. Krissinel, Chem. Phys. Lett. **258**, 283 (1996); E. B. Krissinel and J. Jellinek, *ibid.* **272**, 301 (1997).
[4] G. Rossi, A. Rapallo, C. Mottet, A. Fortunelli, F. Baletto, and R. Ferrando, Phys. Rev. Lett. **93**, 105503 (2004).
[5] D. Sabo, C. Predescu, J. D. Doll, and D. L. Freeman, J. Chem. Phys. **121**, 856 (2004).
[6] F. Calvo and E. Yurtsever, Phys. Rev. B **70**, 045423 (2004).
[7] M. C. Vicéns and G. E. López, Phys. Rev. A **62**, 033203 (2000).
[8] S. Darby, T. V. Mortimer-Jones, R. L. Johnston, and C. Roberts, J. Chem. Phys. **116**, 1536 (2002); M. S. Bailey, N. T. Wilson, C. Roberts, and R. L. Johnston, Eur. Phys. J. D **25**, 41 (2003).
[9] M. J. López, A. Mañanes, J. A. Alonso, and M. P. Íñiguez, Z. Phys. D: At., Mol. Clusters **12**, 237 (1989); M. J. López, M. P. Íñiguez, and J. A. Alonso, Phys. Rev. B **41**, 5636 (1990); A. Mañanes, M. P. Íñiguez, M. J. López, and J. A. Alonso, *ibid.* **42**, 5000 (1990).
[10] A. Bol, J. A. Alonso, J. M. López, and A. Mañanes, Z. Phys. D: At., Mol. Clusters **30**, 349 (1994); A. Bol, G. Martín, J. M. López, and J. A. Alonso, *ibid.* **28**, 311 (1993).
[11] M. D. Deshpande, D. G. Kanhere, P. V. Panat, I. Vasiliev, and R. M. Martin, Phys. Rev. A **65**, 053204 (2002); M. D. Deshpande, D. G. Kanhere, I. Vasiliev, and R. M. Martin, *ibid.* **65**, 033202 (2002).
[12] K. Joshi and D. G. Kanhere, Phys. Rev. A **65**, 043203 (2002).
[13] S. Chacko, D. G. Kanhere, and V. V. Paranjape, Phys. Rev. A **70**, 023204 (2004).
[14] Y. G. Chushak and L. S. Bartell, J. Phys. Chem. B **107**, 3747 (2003).
[15] S. Huang and P. P. Balbuena, J. Phys. Chem. B **106**, 7225 (2002).
[16] K. Joshi and D. G. Kanhere, J. Chem. Phys. **119**, 12301 (2003).
[17] D. S. Mainardi and P. P. Balbuena, Int. J. Quantum Chem. **85**, 580 (2001).
[18] A. Aguado, L. E. González, and J. M. López, J. Phys. Chem. B **108**, 11722 (2004); A. Aguado, S. Núñez and J. M. López, Comput. Mater. Sci. (to be published).
[19] A. Aguado, D. J. González, L. E. González, and J. M. López, in *Progress in Chemical Physics Research* (Nova Science Publishers, Inc., New York, in press).
[20] P. Hohenberg and W. Kohn, Phys. Rev. **136**, B864 (1964).
[21] W. Kohn and L. J. Sham, Phys. Rev. **140**, A1133 (1965).
[22] A. Aguado, J. M. López, J. A. Alonso, and M. J. Stott, J. Chem. Phys. **111**, 6026 (1999).
[23] A. Aguado, J. M. López, J. A. Alonso, and M. J. Stott, J. Phys. Chem. B **105**, 2386 (2001).
[24] A. Aguado, L. M. Molina, J. M. López, and J. A. Alonso, Eur. Phys. J. D **15**, 221 (2001).
[25] A. Aguado, Phys. Rev. B **63**, 115404 (2001).
[26] N. H. March, in *Theory of the Inhomogeneous Electron Gas*, edited by S. Lundqvist and N. H. March (Plenum Press, New York, 1983).
[27] W. Yang, Phys. Rev. A **34**, 4575 (1986).
[28] J. P. Perdew, Phys. Lett. A **165**, 79 (1992).
[29] J. P. Perdew and A. Zunger, Phys. Rev. B **23**, 5048 (1981).
[30] D. M. Ceperley and B. J. Alder, Phys. Rev. Lett. **45**, 566 (1980).
[31] C. Fiolhais, J. P. Perdew, S. Q. Armster, J. M. MacLaren, and M. Brajczewska, Phys. Rev. B **51**, 14 001 (1995); **53**, 13 193 (1996).
[32] R. Car and M. Parrinello, Phys. Rev. Lett. **55**, 2471 (1985); M. C. Payne, M. P. Teter, D. C. Allan, T. A. Arias, and J. D. Joannopoulos, Rev. Mod. Phys. **64**, 1045 (1992).

[33] L. Verlet, Phys. Rev. **159**, 98 (1967); W. C. Swope and H. C. Andersen, J. Chem. Phys. **76**, 637 (1982).
[34] E. M. Pearson, T. Halicioglu, and W. A. Tiller, Phys. Rev. A **32**, 3030 (1985).
[35] M. P. Allen and D. J. Tildesley, *Computer Simulation of Liquids* (Clarendon, Oxford, 1987).
[36] V. Bonacić-Koutecký, J. Jellinek, M. Wiechert, and P. Fantucci, J. Chem. Phys. **107**, 6321 (1997); D. Reichardt, V. Bonacić-Koutecký, P. Fantucci, and J. Jellinek, Chem. Phys. Lett. **279**, 129 (1997).
[37] J. M. Soler, I. L. Garzón, and J. D. Joannopoulos, Solid State Commun. **117**, 621 (2001), and references therein.
[38] J. P. K. Doye, Phys. Rev. B **68**, 195418 (2003).
[39] J. M. Montejano-Carrizales, M. P. Íñiguez, J. A. Alonso and M. J. López, Phys. Rev. B **54**, 5961 (1996).
[40] K. Manninen, H. Häkkinen, and M. Manninen, Phys. Rev. A **70**, 023203 (2004).
[41] E. Aprà, F. Baletto, R. Ferrando, and A. Fortunelli, Phys. Rev. Lett. **93**, 065502 (2004).
[42] J. M. Soler, E. Artacho, J. D. Gale, A. García, J. Junquera, P. Ordejón, and D. Sánchez-Portal, J. Phys.: Condens. Matter **14**, 2475 (2002).
[43] D. R. Hamann, M. Schlüter, and C. Chiang, Phys. Rev. Lett. **43**, 1494 (1979).
[44] L. Kleinman and D. M. Bylander, Phys. Rev. Lett. **48**, 1425 (1982).